JOURNAL OF PROPULSION AND POWER
Vol. 24, No. 4, July–August 2008

Plasma-Assisted Ignition in Scramjets

Lance S. Jacobsen,* Campbell D. Carter,† Thomas A. Jackson,‡ Skip Williams,§ and Jack Barnett¶
U.S. Air Force Research Laboratory,
Wright–Patterson Air Force Base, Ohio 45433
Chung-Jen Tam** and Robert A. Baurle††
Taitech, Inc., Beavercreek, Ohio 45430
and
Daniel Bivolaru‡‡ and Spencer Kuo§§
Polytechnic University, Brooklyn, New York 11201

DOI: 10.2514/1.27358

This study assesses the prospect of main-fuel ignition with plasma-generating devices in a supersonic flow. Progress from this study has established baseline conditions for operation, such as the required operational time of a device to initiate a combustion shock train as predicted by computational fluid dynamics computations. Two plasma torches were investigated: a direct current constricted-arc design and an alternating current unconstricted-arc design based on a modified spark plug. Both plasma torches are realistic in size and operate within the same current and voltage constraints, although differing substantially in orifice geometry. To compare the potential of each concept, the flow physics of each part of the igniter/fuel-injector/combustor system was studied. To understand the constraints involved with the ignition process of a hydrocarbon fuel jet, an experimental effort to study gaseous and liquid hydrocarbons was conducted, involving the testing of ethylene and JP-7 fuels with nitrogen and air plasmas. Results from individual igniter studies have shown plasma igniters to produce hot pockets of highly excited gas with peak temperatures up to 5000 K at only 2 kW total input power. In addition, ethylene and JP-7 flames with a significant level of the hydroxyl radical, as determined by planar laser-induced fluorescence, were also produced in a Mach 2 supersonic flow with a total temperature and pressure of 590 K and 5.4 atm. Information from these experiments is being applied to the generation of constraints and the development of a configuration with perceived high ignition potential in full scramjet combustor testing.

Introduction

THE scramjet engine has no low-speed propulsive capability; it must be boosted to high speed, approximately Mach 4, by another propulsion cycle. There is interest in both hydrogen- and hydrocarbon-fueled scramjet engines for fuel-efficient high-speed flight and space access. Reliable, repeatable ignition of the scramjet at its Mach 4 takeover point is a persistent concern.

Ignition systems used to support ground-test research and development of the scramjet are not readily transferable to in-flight operation. In ground tests, either an aerodynamic or physical restriction of the supersonic flow through the engine is applied to slow the flow through the combustor and raise the static pressure and temperature. This establishes a precombustion shock train in advance of the fuel-injection/flame-holding region. Sufficient heat release in the combustor makes this process self-sustaining, and the starting aid can then be removed. Alternatively, a kinetic accelerant can be used to aid the fuel–air mixture within the engine flowpath to release sufficient heat to backpressure the combustion region. Again, if successful, the starting aid can be removed once combustion is achieved, as the precombustion shock is sustained through combustion heat release with the primary fuel.

The in-flight equivalent of these processes requires incorporation of storage, control, and delivery systems for a secondary supply of gas (thermal and/or aerodynamic blockage) or pyrophoric fluids, such as silane or triethylborane (accelerants). These ignition techniques are effective but increase system weight and complexity and can introduce significant handling/safety issues. Even more onerous, however, is that the reliability and repeatability of these approaches may be inadequate, especially for a reusable system. The ignition process is a transition between blockage introduced for ignition and that resulting from the heat released by fuel–air combustion. Too much backpressure will unstart the engine inlet; too little backpressure fails to achieve the self-sustaining condition. Finally, these approaches permit a small number of engine ignition attempts and probably no restart attempts.

Plasma-based ignition offers a technology alternative for adding large amounts of energy to specific regions of the scramjet flowfield. Duration and repetition of the applied power can be tailored to the ignition requirements. Power supplies can be developed to deliver large amounts of energy for short periods of time. Average power requirements, pulse duration and frequency, and spatial location are all within the designer's control. At issue is whether control over these parameters is sufficient to achieve the self-sustaining condition within the scramjet flowpath at a Mach 4 flight condition or below.

This paper centers on the use of arc plasmas to establish main-fuel ignition with sufficient heat release to form a precombustion shock

Presented as Paper 871 at the 41st Aerospace Sciences Meeting and Exhibit, Reno, NV, 6–9 January 2003; received 17 August 2006; revision received 22 October 2007; accepted for publication 29 October 2007.

*National Research Council Postdoctoral Research Associate, Propulsion Directorate; currently President, GoHYPERSONIC, Inc., 714 East Monument Avenue, Suite 201, Dayton, Ohio. Member AIAA.

†Senior Aerospace Engineer, Propulsion Directorate. Associate Fellow AIAA.

‡Deputy for Science, Propulsion Directorate. Senior Member AIAA.

§Principal Research Physicist, Propulsion Directorate. Senior Member AIAA.

¶Captain, Propulsion Directorate. Member AIAA.

**Senior Research Scientist, 1430 Oak Court, Suite 301. Associate Fellow AIAA.

††Research Scientist; currently Aerospace Engineer, Hypersonic Air-breathing Propulsion Branch, NASA Langley Research Center. Senior Member AIAA.

‡‡Research Scientist; currently Research Scientist, The George Washington University, Washington, D.C. Member AIAA.

§§Professor, Department of Electrical and Computer Engineering, Five MetroTech Center. Member AIAA.

with sufficient strength to make the combustion self-sustaining at Mach 4 flight conditions in a hydrocarbon-fueled scramjet. Our premise is that torch placement relative to fuel-injection sites is the critical parameter in a successful scramjet ignition attempt. Other important variables include the applied power and the plasma feedstock. The investigation is both computational and experimental. In the discussion that follows, the computational approach is outlined and initial results presented. The rest of the paper focuses on the torch technology and the interaction of the torch and a fuel injector in a supersonic flowfield.

Arc-type plasma ignition devices have been a topic of interest in the study of supersonic combustion for over 20 years [1–7]. This has been the most common type of plasma investigated in supersonic crossflows due to the relative maturity of the technology in high-pressure environments. The arc discharge device discussed in this paper is a plasma torch, in which the arc is coupled to a stream of gas. This device is compact and provides a source of hot, thermal energy with an abundance of excited and ionized species. Its configuration permits localized variation of position of the plasma jet along the walls of a combustor, which, with proper placement, could be used to ignite, hold, and potentially enhance combustion [8].

Conditions inside the scramjet combustor do not favor autoignition at Mach 4 or below for either hydrogen or hydrocarbon fuels and do not necessarily get better with increasing flight Mach number. In addition, fuel selection plays a significant role in the ignition process. Limited work has been published in this area, with the focus predominantly on hydrogen and light hydrocarbons. Near Mach 4 flight conditions, examples of the influence of engine fuel on ignitability are shown in Fig. 1. This figure consists of experimental scramjet ignition data published by several different authors (see also Table 1). The data in this graph show reported minimum ignition powers required by plasma-torch igniters used to ignite hydrogen, ethylene, ethane, and methane fuels in various scramjet combustor configurations with freestream Mach numbers ranging from 1.8 to 2.5. Also shown in this figure (dashed line) is a typical value of combustor air total temperature at Mach 4 flight conditions (∼910 K), with a combustor Mach number of 2.0. Here, the Mach 4 flight combustor total temperature is based on output from the ramjet performance analysis code (RJPA) [18], from an adiabatic inlet at an altitude of 22 km with a dynamic pressure of 0.5 atm (1000 psf) and a combustor Mach number of 2.0 [19]. Clearly, there have been successful plasma ignition experiments at Mach 4 flight conditions for scramjet combustors fueled by hydrogen and ethylene.

Before discussing the data presented in Fig. 1, it is important to come up with a general definition for successful ignition in a supersonic combustor. Throughout the works cited in this document, the definition changes slightly, depending on the available experimental tools. In addition, the typical total temperatures required for ignition in a practical scramjet, in general, are below the autoignition limits of the combined fuel and combustor configuration. Typically, ignition has been documented by visible plume emission [2,3], the output from pitot and total temperature probes [1], and increases in the wall pressure [2,3,14,19] and/or wall temperature [9,10,13]. The concept of global ignition must also be introduced, because in all of the plasma-torch configurations involving nearby fuel, there will generally be some degree of fuel–air combustion near the plasma-torch effluent. Global ignition is defined here as ignition that spreads a flame throughout the length and intended area of the combustor and produces enough heat release to generate a shock train throughout the axial length of the combustor. This may be measured by a continual pressure or temperature rise throughout the length of the combustor. With this definition, successful ignition does not imply that there has been a sufficient level of heat release necessary to thermally choke a combustor duct, but rather enough to separate the wall boundary layer and sustain a shock train while propagating a flame throughout the combustor volume.

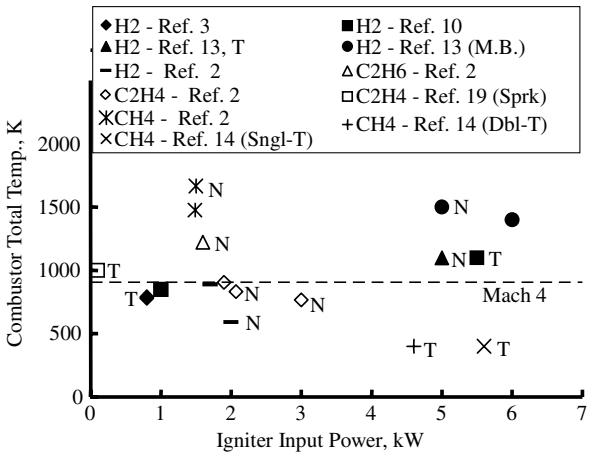

Fig. 1 Global ignition in scramjets with different engine fuels; *N*: net input power; *T*: total input power.

In an interesting example of local ignition, Masuya et al. [15] have demonstrated that it is possible to sustain a shock train in a small (3.0×3.0 cm) duct having no step (or cavity) at low pressure and temperature (see Table 1) by the use of a plasma torch. In this set of experiments, the feedstock from the plasma torch was a 50/50 mixture of hydrogen and nitrogen (by volume) producing an overall combustor equivalence ratio of 0.009 with no other source of fuel. Combustion in this experiment was only reported in the vicinity near the plasma-torch jet, and the flame was reportedly quenched due to the low temperature in the duct. Global ignition is presumably not achieved here, due to the very low equivalence ratio and quenching.

In experiments described by Northam et al. [2] with ethane and methane fuels (cross-sectional dimensions of 8.9×3.8 cm), the minimum combustor total temperatures were far above the required level of 910 K (dashed line) for Mach 4 flight. However, Shuzenji et al. [14] have also had success in igniting a small methane-fueled supersonic duct (having cross-sectional dimensions of 3.0×2.0 cm and a 0.5 cm backward-facing step) at very low total temperature (400 K). Although the results of Shuzenji et al. are impressive, a small combustor having no divergence is presumably easier to ignite with the typically used plasma powers than a larger combustor. To date, no experimental work has been published involving the ignition of liquid hydrocarbon fuels without the use of a downstream backpressure generating device (aerothrottle) or silane (accelerant).

Other points of interest in Fig. 1 are the $H_2 + O_2$ microburner (MB) used by Kobayashi et al. [13] and the double-torch configuration (Dbl-T) shown by Shuzenji et al. [14]. In both of these studies, the performance of the two devices was compared with those using single plasma-torch igniters. Masuya et al. [10] have also examined the influence of cross-stream duct placement on the ignitability of a scramjet combustor. These authors concluded that placing the plasma torch in addition to adding a step on the small length of their combustor (14.7×3.2 cm cross dimensions) significantly reduced the required input power as well as the total temperature for ignition.

Scramjet combustors are typically designed with emphasis on flame holding and efficient combustion. Usually ignition concepts are then integrated into the engines afterward, so that the problem becomes one of how to ignite the particular combustor. Along these lines, it may be beneficial to alter particular aspects of proven combustor geometry, such as the location of fuel relative to flame holding mechanisms, or to add subsonic areas (e.g., a step, as was done by Masuya et al. [10]) to provide the heat release necessary to initiate and spread main-fuel combustion. The point here is that a design with adequate flame holding may be inadequate for a particular ignition strategy.

To obtain a better understanding of the differences between sufficient conditions for flame holding and ignition, it is useful to examine the work done by Mathur et al. [19]. In this study, combustion experiments were performed in an uncooled combustor of rectangular cross section with four low-angled ethylene-fueled injectors arranged in a cross-stream row, just upstream of a cavity flame holder. The cavity flame holder was lit with a spark plug and intense combustion was achieved over a wide range of equivalence ratios at a combustor total temperature of 1000 K. In one test case, after main combustion was achieved, the total temperature was

Table 1 Plasma-assisted ignition experiments

Authors	Combustor inlet cross dimensions, cm	Step height, mm	Mach no.	P_t, atm	P, atm	T_t, K	Eqiv. ratio	Igniter feedstock	Input power, kW	Downstream configuration order
Kimura et al. [1],[b]	2.5×3.3	——	2.1, 2.7	9.2, 30	1	290, 450	~0.1, ~0.07	H_2, N_2, Ar	4.7[h,i],	Fuel/fuel/torch/fuel
Northam et al. [2],[b,c,d,e]	8.9×3.8	3.8×2[f]	2[a]	8	1	590–1800	0.16–0.47	Ar + H_2	1.5–3.4[h,i]	Step/fuel/torch/fuel
Wagner et al. [3],[b]	8.9×3.8	3.8×2[f]	2[a]	8	1	780–1560	0.28	Ar + H_2	0.5–2.6[i,k]	Fuel/step/torch fuel
Sato et al. [9],[b]	14.7×3.2	3.2×2[f]	2.5[a]	10	0.6	1000–2500	0.1–0.8	O_2, N_2, Air, Ar + H_2	3.2[i,j]	Torch/step/fuel
Masuya et al. [10],[b]	14.7×3.2	3.2×3[f]	2.5[a]	10	0.6	800–2500	0.4–0.8	O_2, Air	1–5.5[i,j]	a) Torch/step/fuel b) Fuel/torch/fuel/fuel c) Fuel/torch/cavity w/fuel
Tomioka et al. [11],[b]	25×6.7	4.0×2[f], 2.0×1[f]	2.6, 4. 1, 5.3[a]	9.3, 55, 100	0.45, 0.25, 0.09	890–2600	0.1–1.0	O_2	1 − 1.5 × 2	a) Fuel/torch/step b) Fuel/torch/cavity w/fuel c) Fuel/torch/step + strut
Masuya et al. [12],[b]	3.0×3.0	——	1.8	1	0.17	290	0.013	O_2, N_2, N_2 + H_2	1.5–6[i,j]	Fuel/fuel/torch/fuel
Kobayashi et al. [13][b]	14.7×3.2	3.2×2[f]	2.5[a]	10	0.6	800–2500	0.4	O_2, (H_2 + O_2[g])	1–5.5[h,i], (1–45)[h,k]	Torch/step/fuel
Shuzenji et al. [14],[e]	3.0×2.0	5×1[f]	2	3.8	0.5	400	0.16	Air	4–6[i,k]	Fuel/torch/torch/step
Masuya et al. [15],[b]	3.0×3.0	——	2.3	1	0.17	273	0–~0.009	He, N_2, N_2 + H_2	1.5–6.3[i,j]	Torch only
Bonanos et al. [16][b,c]	2.5×3.8	——	2	3.25	0.4	1100	0.1–0.5	N_2, Air	3.7[b], 5.2[c], 8.9[c,i,k]	Fuel/torch/torch/torch
Bonanos et al. [17],[b],[c]	2.5×3.8	——	2	3.25	0.4	1100	0.1–0.5	Air	3.5[b], 6.1[c,i,k]	Fuel/torch/torch/torch

[a]$H_2 + O_2$ vitiated air.
[b]H_2 fuel.
[c]C_2H_4 fuel.
[d]C_3H_6 fuel.
[e]CH_4 fuel.
[f]Number of combustor walls with steps.
[g]Used $H_2 + O_2$ microburner as comparison to plasma torch.
[h]Net power.
[i]Total power.
[j]water cooled,
[k]uncooled,

reduced to 944 K and vigorous combustion was maintained. During another test with this configuration, an attempt to start the combustor at 944 K was made over a wide range of fuel pressures with no success. Clearly, the combustor conditions were not sufficient to produce the combustion shock train, and the flame from the cavity could not spread into the main duct. This implies that the heat release rate (of the main-fuel jets) must be sufficiently high to allow flame spreading away from the cavity, thereby raising the combustor pressure and initiating a shock train. Indeed, Northam et al. [2] showed that it was possible to reduce the required total temperature from 1000 to 770 K in an ethylene-fueled configuration with an integrated backward-facing step and a plasma torch operating at 3 kW.

An example of the influence of flight Mach number and combustor geometry on a plasma-assisted ignition system is described by Tomioka et al. [11]. In this study, a complete hydrogen fueled scramjet engine was tested in a freejet facility, simulating flight Mach numbers of 4, 6, and 8; freestream air was heated with a storage heater at the Mach 4 and 6 conditions and with a hydrogen/oxygen vitiator at the Mach 8 condition. The configuration included a step that was directly connected to additional steps on the sidewalls of the combustor, which helped to spread the flame around the combustor perimeter. Two oxygen-fed, plasma-torch igniters using 1–1.5 kW of input power, were used to ignite the combustor. It was found that with the original configuration, in which the two plasma torches were placed on the top wall 20 mm upstream of a backward-facing step, ignition of the engine was achieved only at Mach 4. To attain ignition at the Mach 6 condition, a cavity was incorporated into the region from the top wall step (making it deeper) to 40 mm downstream, and then oxygen was injected into the step region. This configuration provided only limited ignition, and the flame did not spread laterally throughout the combustor. Global ignition of the main-fuel flow with this configuration was possible only when the main-fuel flow rate was increased to a high level, which consequently increased the pressure in the base of the step region, allowing more vigorous combustion. This meant that the ignition condition was restricted to a small range of combustor equivalence ratios. At this point, to ensure a wider operational range, a short strut was added into the combustor flowpath (mounted from the center of the top combustor wall) with a height one-fifth of the engine height. This strut was introduced with the sole purpose of increasing the pressure at the base of the flame-holding steps (the cavity recess on the top wall and the auxiliary oxygen injector were removed from this configuration). This configuration successfully widened the operational range, with respect to overall engine equivalence ratio, at the Mach 6 condition. However, the pressure in the step regions was still not sufficiently high to ignite the engine at the Mach 8 flight condition.

Modeling the Ignition Process

The use of computational fluid dynamics (CFD) is of paramount importance to aid in the establishment of system guidelines and to simplify the process of igniter placement in a scramjet combustor. Furthermore, the combined experimental–computational approach allows interaction through each step of the process. Starting with individual igniter evaluation, experiments help validate the models used to simulate the plasma discharge. This, in turn, improves the confidence in the computational effort when a crossflow, fuel, and an igniter are combined. Furthermore, calibration of CFD routines with combined flow experiments help to reduce and guide the experimental test matrix required when studying an igniter concept.

One insightful example of how CFD has been used to define the ignition problem in relation to the use of plasma torches in a full engine configuration is shown in the following calculations performed with the VULCAN [20] (viscous upwind algorithm for complex flow analysis) software package. This routine solves the Reynolds-averaged conservation equations for mixtures of thermally perfect gases using a cell-centered finite volume scheme. Furthermore, the low-diffusion flux split scheme (LDFSS) of Edwards [21] was used. A time-accurate integration was required once the plasma torches were activated to assess the ignition characteristics. The simulations were performed using an implicit dual time-stepping algorithm that combines a diagonalized approximate factorization scheme to integrate in pseudotime, with a three-point backward finite-difference approximation for integration in real time. This scheme provides the desired second-order temporal accuracy without a stringent time-step restriction based on numerical stability. All time-accurate simulations were performed with a constant time step of 0.1 μs.

The geometry of the injectors, cavity, and plasma torches simulated in this study are shown in Fig. 2. A schematic of the combustor rig flowpath considered in this investigation is shown in Fig. 3. The modeling assumptions for the plasma fluid employed in the CFD simulations neglect many important effects [magnetohydrodynamics (MHD), ionization, etc.] that are likely to enhance the ability of the plasma to ignite the flow. In this study, the decision was made to ignite the flow within the cavity flame holder before the initiation of plasma into the system. This would provide a relatively large pool of hot combustion products, including radicals, to aid the plasma torches in igniting the flow. The calculations used a 10 reaction, 10 step mechanism to simulate ethylene combustion in air [22]. Though adequate for some steady-burning problems, this kinetic mechanism was unable to simulate cavity combustion at the Mach 4 flight condition (the cavity would not remain lit), though, in fact, the cavity reactants will ignite, using just spark plugs, and readily burn under these conditions. Consequently, to better match the observed cavity flame-holding behavior, the reaction rates were increased by a factor of 10 and the cavity surfaces were preheated to a temperature of 3000 K. This approach enabled robust combustion within the cavity. More recently, Liu et al. [23] have introduced a reduced ethylene–air combustion chemistry mechanism with much improved fidelity; of course, computation times are also much greater with this mechanism. In this paper, the plasma-torch plume was modeled as an enthalpy source consisting of equilibrium air consisting of O_2, O, and N_2 (nitrogen chemistry was not included in the mechanism) at a temperature of 3400 K. Two injector hole diameters were modeled, 3.18 and 1.59 mm, simulating 10 and 2.5 kW of net input power, respectively, for the two hole sizes. Both sets of plasma-torch boundary conditions produced similar computational results, and so only the 2.5 kW computational result is discussed next.

The time history of the scramjet ignition process is shown in Fig. 4 in the form of temperature contours. The elapsed time between each image is 0.3 ms. After 0.3 ms, the lower portion of the fuel plume is starting to ignite. The combustion is somewhat more intense near the combustor sidewall, but, overall, the ignition process is relatively uniform over the entire combustor span. At 0.6 ms, the flame has spread around the periphery of the fuel plumes, and the heat release is forcing the combusting fluid toward the cowlside surface (opposite of the cavity side). At 0.9 and 1.2 ms, the combustion front has expanded to fill the entire cross-sectional area of the combustor just downstream of the cavity flame holder. The flame structure at this

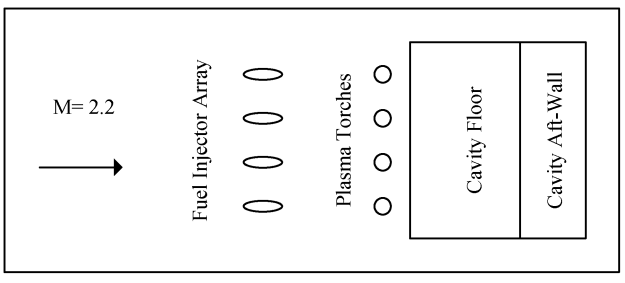

Fig. 2 Injector/cavity configuration with simulated plasma torches.

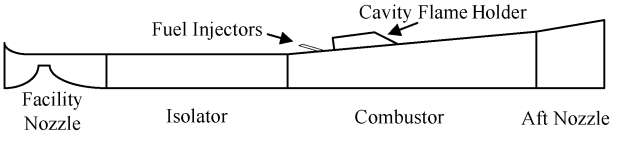

Fig. 3 Simulated scramjet combustor flowpath.

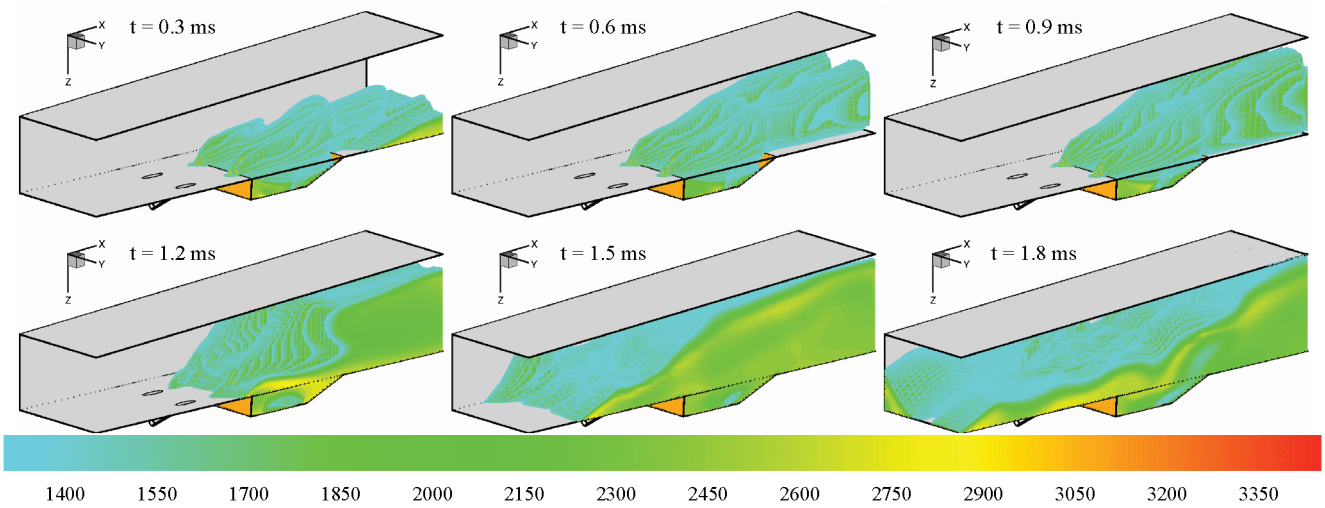

Fig. 4 Temperature contours (Kelvin) describing the ignition process in a scramjet combustor (evolving in time steps of 0.3 ms, from left to right starting at the top left corner) using a simulated plasma-torch igniter operating at 2.5 kW each. Two igniter positions are shown in the top contours for these half-combustor simulations based on symmetry of the combustor.

point is still relatively symmetric. The influence of the precombustion shock train that has formed due to the heat release of combustion is clearly seen at 1.5 and 1.8 ms. At this time, the combustion front has moved upstream of the fuel-injection ports, due to flow recirculation caused by shock/boundary-layer interactions. The precombustion shock train has also caused an asymmetry to develop near the sidewall/bodyside juncture. This corner region has a relatively large volume of low-momentum flow, which tends to separate more readily than the thinner, attached boundary layer that exists on the remaining sections of the combustor surface.

Despite the utility of CFD to assess the ignition process, the current computational methods are still too limited to rely upon as a sole method of analysis. Because of the necessity of greatly simplified reduced kinetics, simplified equations of motion, and the approximated turbulence modeling in the Reynolds-averaged Navier–Stokes (RANS) computational analysis, CFD currently is used as a guideline to help develop experimental directions and refine experimental test matrices.

Plasma-Torch Igniters

The two plasma torches under investigation in this study are a dc constricted-arc design [24] and an ac unconstricted-arc design [25].

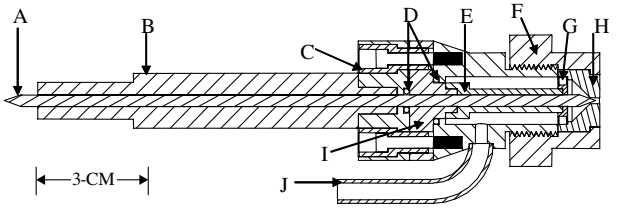

Fig. 5 DC plasma-torch igniter: A) cathode, B) Starrett 440 depth micrometer head, C) PEEK screw insulator, D) O-rings, E) Macor ceramic support rod, F) anode housing, G) Macor ceramic flow swirler, H) copper anode, I) PEEK insulator, J) feedstock tube.

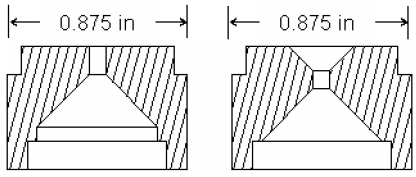

Fig. 6 DC plasma-torch anodes with 0 deg, sonic (left) and 45 deg, divergent constrictor angle (right).

Hereafter, these will simply be referred to as the dc and ac plasma torches. Prototypes were built and an evaluation of their general characteristics and power utilization was accomplished. Both igniters have been evaluated in a quiescent ambient environment. The primary objective here is to understand the operational and physical characteristics involved with each design. Once the flow physics of a design are understood, advantages, disadvantages, and operational modes of interest can be established.

Design

Figures 5 and 6 show drawings of the dc plasma torch and its two anode geometries [24]. The dc plasma-torch design consists of a constricted arc with a 1.59 mm throat diameter d_t. Figure 7 shows a drawing of the ac plasma torch with a 6.4 mm outer jet exit diameter and its feedstock plenum design for insertion into a supersonic facility, discussed later in the paper. Both torches use a central tungsten electrode. This piece functions as the cathode in the dc torch and alternates as both anode and cathode in the ac design. The dc torch is designed for flow rates ranging from 10 to 80 SLPM (standard liters per minute, referenced to STP, i.e., 40 SLPM of N_2 equals 0.83 g/s) of air or nitrogen, whereas the ac design can be operated from 0 to 1500 SLPM, the feedstock exit being choked at roughly 500–600 SLPM, depending on the backpressure of the environment. An example of the current and voltage traces produced by both torches is shown in Fig. 8.

In this report, only total input power is reported, because the steady-state thermal efficiency of the dc plasma torch was determined to be $\geq 95\%$ with the sonic anode geometry [24]. Because of the nature of operation of the ac design, for example, that

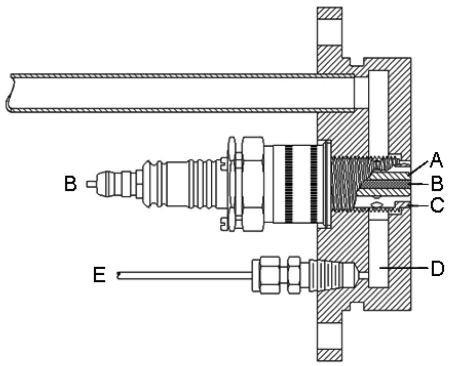

Fig. 7 AC plasma-torch igniter: A) ceramic insulator, B) inner electrode, C) outer electrode, D) plenum chamber, E) feed stock tube.

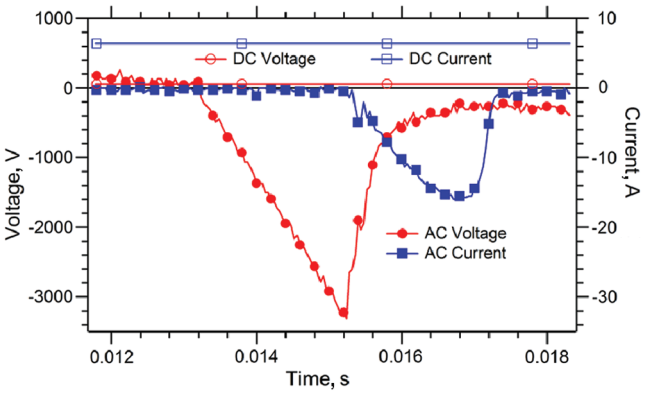

Fig. 8 Current and voltage traces for the dc (top) and ac (bottom) plasma torches.

its arc runs past the physical body of the torch (and is enveloped in the torch feedstock), the thermal efficiency of this design is also expected to be near unity.

Flow Characteristics

Figures 9a and 9b show schlieren images taken with the dc and ac plasma-torch igniters, respectively, both with nitrogen feedstock in a quiescent, ambient environment. The schlieren images were taken with a Princeton Scientific Instruments high-speed camera capable of recording 32 images at rates up to 1 million frames per second. The images show some of the differences associated with the two plasma torches in operation. With both torches, an arc can be seen to emerge from the torch exit and penetrate vertically into the jet. However, due to the differences in the configurations of the two torches involving flow rates, injector exit diameters, and voltage-current operational characteristics, the two flowfields have very different characteristics: a narrow, constant jet with the dc-torch design and a wide, pulsating jet in the ac-torch design. Note that the flow rate range is 1 order of magnitude higher for the ac design than the dc design.

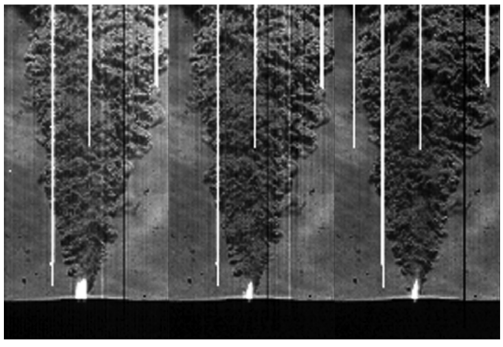

a) DC plasma torch with sonic anode (Interframe times = 0.1, 0.2, 0.4 ms, left to right)

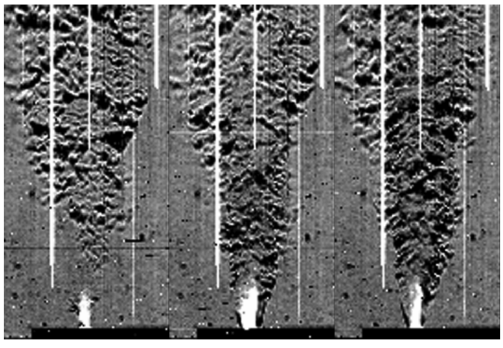

b) AC plasma torch (Interframe time = 2 ms)

Fig. 9 Schlieren images of dc and ac plasma-torch igniters (image size 9.9 × 5.0 cm).

The ac-torch arc-voltage characteristics provide an arc with a voltage of about 400 V at its peak power in the cycle, which for an equivalent peak power to the dc torch, produces an arc length about four times as long for a quarter of the required current. One further note of interest regarding behavior of the ac torch is that for the estimated ignition period of about 2 ms, the torch behaves like a dc device, in that each pulse in its ac cycle is 1/120th of a second long (∼8 ms), so that the peak power portion of each pulse, ∼2 ms, is comparable to the required time necessary for the ignition process in a scramjet based upon the CFD results. This was an intentional design feature. The time scales in the two sets of selected images were chosen as follows: for the dc torch, 0.1, 0.2, and 0.4 ms interframe times (from left to right), and for the ac torch, equal 2 ms interframe times. The variable interframe times of the dc torch allows one to observe the structures in the region near the arc and to obtain some understanding of the dynamics between the motion of the arc and the reaction of the plasma jet plume. The 2 ms interframe time for the ac torch shows the characteristics of a single pulse in its ac power cycle.

In Fig. 10, results are shown from nitric oxide planar laser-induced fluorescence (NO-PLIF) probing of the dc plasma torch in operation with a nitrogen feedstock (40 SLPM) at total input power levels of 1 and 2 kW. These instantaneous images illustrate the various levels of NO concentration ranging from blue (low) to red (high). A detailed description of the NO-PLIF experiments is presented in Jacobsen et al. [24]. It is noted that the NO-PLIF images have not been corrected for variations in electronic quenching rate, Boltzmann fraction, or laser sheet irradiance profile. The hoop structure of the arc

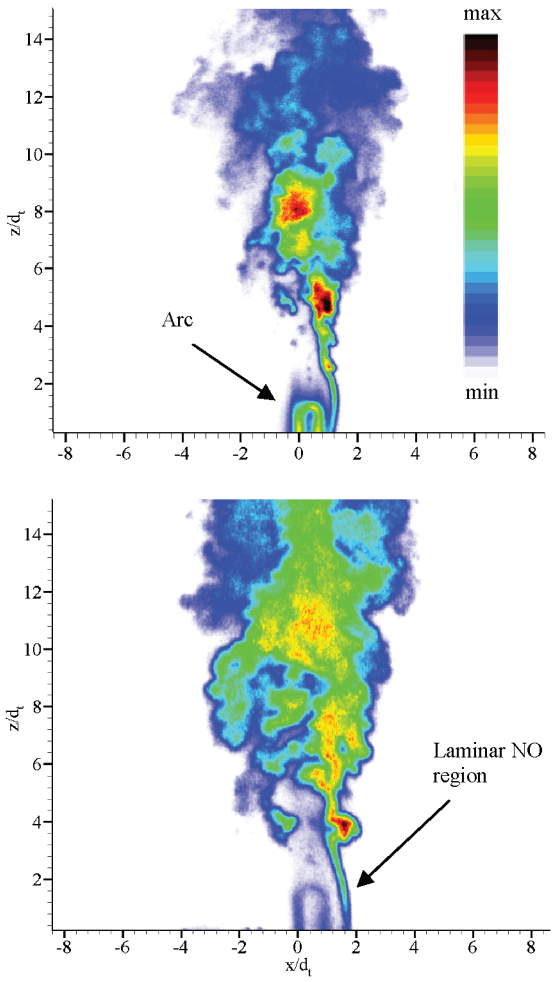

Fig. 10 False-color instantaneous NO-PLIF images of dc plasma torch in an ambient environment. Top: sonic anode, 40 SLPM N_2, 1 kW. Bottom: sonic anode, 40 SLPM N_2, 2 kW.

is especially clear in these images (see [25] for a similar image with the ac torch), and, in both, the arc exits the plasma-torch sonic orifice on the left side of the arc hoop and impacts on the torch anode to the right. A laminar region to the right of the hoop marks the region where the ambient air in the test section is being entrained into the plasma jet and reacts with the plasma jet to form NO. A transition to turbulence can be seen at the top of the laminar structure, marked by the unsteady, high-signal-intensity NO region. Two regions of high-NO fluorescence are shown at the centerline of the images and to the right in the aforementioned entrainment region. It is interesting to note that the NO profiles, in a steady-state sense, reach a near symmetric state past 11 torch throat diameters d_t downstream of the torch exit.

An instantaneous image pair of NO-PLIF and temperature, derived from a filtered Rayleigh scattering (FRS) measurement, is shown in Fig. 11 [24]. In some locations, scattering from particles that originate from the electrodes (near the arc attachment point) "bleeds" through the iodine filter. These high-signal regions (from particle scattering or arc emission) were set to 0 K (white in the color table) using a threshold filter. The rough outline of the NO profile from the first image in Fig. 11 is overlaid on top of the temperature image to indicate the relationship between the hot-temperature pockets created by the arc heating process and the formation of NO by the entrainment of air into the nitrogen plume. In these images, it is evident that the locations of high-NO signal correspond well to the temperature region between 900 and 1300 K; of course, the high-signal regions reflect a complex mixing and reaction process. It is noteworthy that in Behbahani et al. [26], the hot-gas pockets were postulated to be from the thermal stratification of the plasma jet, causing the arc to heat only a small portion of the jet to exceedingly high temperatures. An example of this is shown in Fig. 11: a pocket with $T \approx 3600$ K is seen just downstream of the arc hoop. In some cases, at 2 kW total input power, peak temperatures can exceed 5000 K.

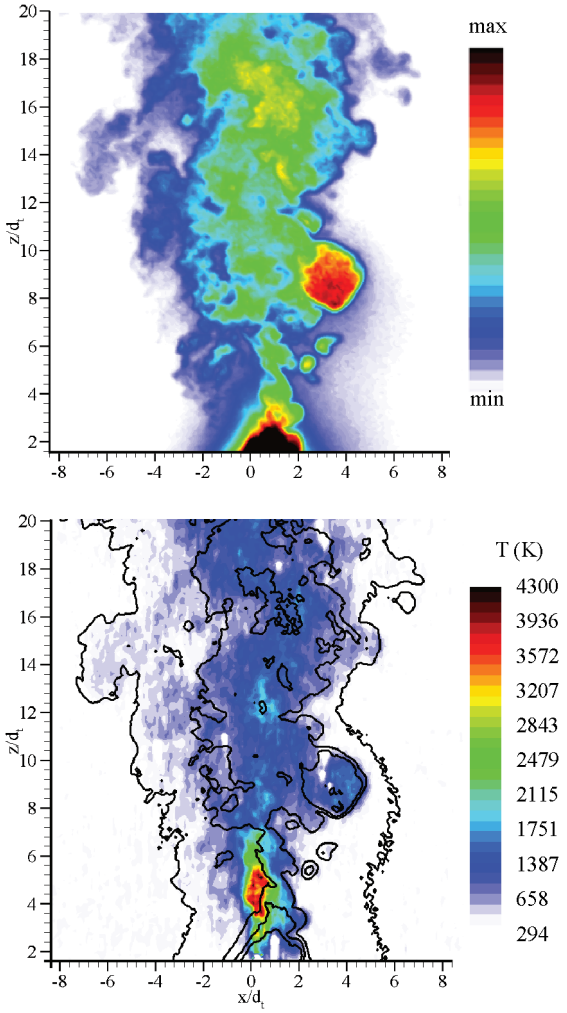

Fig. 11 Simultaneous false-color images showing the effluent of the dc plasma torch with a divergent anode, 20 SLPM N_2 and 2 kW input power. Top: NO-PLIF image. Bottom: temperature image with superimposed NO field. In the NO-PLIF image, the black region at the bottom corresponds to emission from the arc that saturated those camera pixels.

Torch/Fuel-Injector Interaction: Experiment

Critical to the success and utility of plasma-assisted ignition is the interaction of torch and fuel-injector plume. Following the characterization of both torches in a quiescent environment, combined fuel and igniter testing in supersonic flows was conducted. At the most basic level, the torches under investigation exhibit insufficient momentum to significantly penetrate the boundary layer into the supersonic flow, characteristic of the scramjet. The momentum of the fuel plume, however, is sufficient to transport plasma to the fuel-plume core and also to the near-stoichiometric mixing region around the plume to influence more of the reactants.

Experimental Setup

Initial evaluation was conducted in a supersonic, Mach 2 facility at the U.S. Air Force Research Laboratory (Wright Patterson Air Force Base). Tests were run at two different total temperatures: 300 and 590 K; the latter value was limited by the type of seals used in the tunnel walls. As noted, at a Mach 4 flight condition, the total temperature would be considerably higher (by ~300 K). This facility allows testing of an individual concept with both gaseous and liquid hydrocarbon fuels in the absence of a cavity-based flame holder. A sketch of the plasma torch and flush-wall injector inserts is shown in Fig. 12. This 15.2 × 30.5 cm test section floor plate fits into a simulated scramjet combustor duct with an initial duct height of 5.1 cm with a uniform inflow from the nozzle; the measured Mach number is 1.94. At the upstream edge of the test section insert, the simulated combustor section diverges on the injector side by 2.5 deg. This particular hardware was intentionally designed not to study global ignition, as such, but to reduce the chance of causing global ignition by maintaining the overall equivalence ratio of the tunnel below 0.1. In addition, the fuel injector was placed at the centerline of the tunnel without any flame-holding mechanisms, such as a cavity or backward-facing step. In this way, one can study the interactions of the fuel plume with the plasma torch by itself, and any flame produced is strictly created by this interaction (hence decoupling the

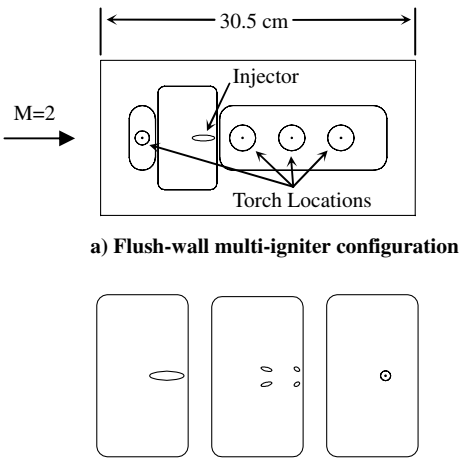

a) Flush-wall multi-igniter configuration

b) Fuel-injector inserts. From left to right: Single 15-deg hole, Aeroramp, aerated liquid

Fig. 12 Test hardware for combined fuel and igniter experiments without a cavity-based flame-holding system.

ignition and flame-holding problems as much as possible from the combustor geometry).

The three injectors used in this study were 1) a single 5.61-mm-diam, 15 deg downstream-angled hole, 2) an aeroramp injector with an equivalent jet diameter of 4.76 mm (similar to the one described in Jacobsen et al. [27]), and 3) an aerated-liquid injector having a 1.59-mm-diam exit hole and designed for normal injection into the crossflow. Included in this work are data using the first two downstream plasma-torch locations (see Fig. 12): station 1 was located 38.1 mm downstream from the center of the gaseous injector holes (see Jacobsen et al. [6]); station 2 was located 47.6 mm further downstream from station 1.

During the experiment, a wide range of fuel flow rates was investigated. It was found that a flame of significant length could produced only when the injectors were operated at very low flow rates relative to the size of the injectors. Because of this, the maximum fuel flow rate reported here is nominally 5.4 g/s, which corresponds closely to a matched-pressure condition with a jet-to-freestream momentum-flux ratio of 0.22 (duct divergence not accounted) for the aeroramp injector.

Flame Diagnostics

The two major flame diagnostics used in this study were chemiluminescence imaging (using a standard 30 Hz video camera) and OH planar laser-induced fluorescence (OH-PLIF). The OH-PLIF technique was used to assess the degree of combustion at specific downstream locations; in all cases, there was qualitative agreement between the OH-PLIF signal strength (counts) and the chemiluminescence plume emission. However, using solely chemiluminescence to compare the ac- and dc-torch performance in generating the flame plume can be misleading because of the pulsed nature of the ac torch (not synchronized with the camera) and the autoexposure feature of the video camera.

The OH-PLIF measurements were accomplished with a Lumonics Hyperdye HD-300 dye laser that was pumped with the second harmonic of an injection-seeded Spectra Physics Nd:YAG laser (GCR-170). The dye laser was tuned to 587 nm so that when frequency doubled, using an Inrad Autotraker III, the wavelength matched that of the $Q_1(8)$ transition of the $A^2\Sigma^+ - X^2\Pi$ (1, 0) band for OH. The resulting pump beam line width was $\sim$0.1 cm^{-1}. To ensure good overlap of the laser and transition, a portion of the UV beam was split off and directed over a small reference flame and then to a fast photodiode. A pair of lenses collected and focused the resulting laser-induced fluorescence onto the photocathode of a photomultiplier tube. This signal, along with the photodiode output, was continuously displayed on an oscilloscope, allowing minor adjustments to be made to the dye laser grating position to mitigate the effects of laboratory temperature changes.

The transmitting and receiving optical hardware were positioned on a traversing table, allowing remote positioning of the measurement volume at any desired station in the flowfield. The laser sheet was formed using a pair of lenses, a plano-concave cylindrical lens with -150 mm focal length and a plano-convex spherical lens with 1000 mm focal length. This arrangement resulted in a sheet width of about 50 mm. This sheet was directed across the span of the test section through the fused silica side window; the resulting fluorescence was imaged off-axis to the sheet normal using a Princeton Instruments PIMAX "Superblue" intensified charged-coupled device (ICCD) camera having a 512×512 pixel array. The camera was fitted with a 105 mm, f/4.5 UV-Nikkor lens, and UG-11 and WG-295 Schott glass filters, allowing transmission of fluorescence from the OH A–X (0, 0) and (1, 1) bands. Image blur, the result of off-axis imaging, was effectively mitigated by binning the pixels 3×3. Perspective distortion, also a consequence of the off-axis imaging, was corrected by imaging an array of dots (a dot card) and using locations of "corner" dots as inputs to the MATLAB *Projective* algorithm. Strong emission from the plasma torches was suppressed through the use of a UG-11 Schott glass filter (blocking visible radiation) and through intensifier gating (150 ns gate width). The background emission, especially in the UV, was suppressed further by gating of the intensifier microchannel plate voltage in a process called bracket pulsing.

For the ac-torch testing, three pieces of equipment, the plasma-torch system, the laser system, and the ICCD camera, were synchronized to detect the OH fluorescence at the desired time. Note that timing synchronization with respect to the dc torch was not necessary. The ac torch operates at 120 Hz with two effective arc cycles per 60 Hz ac cycle. In one arc cycle, the anode is the center electrode and the cathode is the electrode body. In the next arc cycle, the anode and cathode are switched. The arc timing varies by $\pm$0.5 ms (because the initiation of the arc is highly dependent on local conditions and thus does not occur along the same path), leading to some shot-to-shot variation in OH-PLIF signal. Timing of the camera and laser with respect to the 120 Hz arc cycle was accomplished with a Quantum Composer 9318 pulse generator; with this device, OH was probed on every 12th arc cycle, so that the laser repetition rate could remain at 10 Hz, and any particular phase of the ac-torch cycle could be probed. The average OH-PLIF intensity images correspond to specific phase delays, accurate to within $\pm$0.5 ms of the arc initiation.

Flame Plume Chemiluminescence Video Images

A sample set of flame chemiluminescence images is shown in Fig. 13. Here, both the ac (Figs. 13a and 13b) and dc (Figs. 13c–13f) plasma torches (sonic anode) are shown in operation at station 2, and ethylene is supplied from either the single-hole (Fig. 13a) or aeroramp (Figs. 13b–13f) injector. The images are sequentially arranged so that one main parameter is different from one image to the next: (Fig. 13a) single hole – (Fig. 13b) aeroramp; (Fig. 13b) ac plasma torch – (Fig. 13c) dc plasma torch; (Fig. 13c) air feedstock – (Fig. 13d) N_2 feedstock; (Fig. 13d) 5.4 g/s C_2H_4 – (Fig. 13e) 3.3 g/s C_2H_4; (Fig. 13e) 586 K freestream total temperature – (Fig. 13f) 305 K freestream total temperature.

The most noticeable features shown in this image sequence are that the dc torch produced a larger visible flame than the ac torch (images in Figs. 13b and 13c), for the same fuel flow rate and approximate power (measured at/near the peak of the waveform for the ac torch). Of course, with the ac torch, the instantaneous power level and flame intensity fluctuate at 120 Hz. The ac-torch images presented here were the brightest flame images, selected from the 30 Hz video recordings, and no attempt was made to synchronize the 30 Hz acquisition with the 120 Hz arc frequency for maximum power. Several feedstock flow rates were tried with the ac torch over its operational range (0–1500 SLPM air) and a flow rate of $\sim$250 SLPM air was determined to produce the longest visible flame for its current electrode configuration. Air produced a longer flame when compared with nitrogen as the torch feedstock with the dc torch (images in Figs. 13c and 13d). However, control of the dc torch with air was more difficult due to high cathode erosion rates [note, power levels between Figs. 13c and 13d are different by 0.9 kW (the case with air being higher)] and, consequently, only a limited set of data is available for comparison. The difference in flame size in Figs. 13c and 13d could also indicate that this type of flame is very sensitive to the local equivalence ratio and coupling of the ignition source with the mixture. In general, with the dc torch, as the fuel flow rate was reduced, the flame length grew (Figs. 13d and 13e) and extended throughout the length of the combustor. When the freestream temperature was reduced, the flame diminished in intensity, though it is interesting to note that the length of the flame was still substantial (Figs. 13e and 13f). A general comparison of the single-hole and the aeroramp injectors (Figs. 13a and 13b) is also shown, although, to-date, an insufficient number of tests have been conducted with the single-hole injector to assess its performance relative to that of the aeroramp.

OH Planar Laser-Induced Fluorescence

OH-PLIF was used as a diagnostic because OH is a reasonable reaction progress marker. Spanwise OH-PLIF images were recorded at two downstream locations, both 5.1 cm downstream of the plasma-torch exit for either station 1 or station 2 (noted for torch station 1 by

the red dashed line on the video still image in Fig. 13c); thus, the OH probe location was a fixed distance from the plasma-torch exit but varied with respect to the fuel-injection location. This OH probe location was chosen, in part, to mitigate interference (for the OH-PLIF) from the torch plume, and the OH images presented here correspond to the test configuration with the aeroramp injector and stations 1 and 2. Only a limited number of tests were devoted to the single-hole (ethylene) and aerated-liquid (JP-7) injectors. The OH-PLIF intensities generated with these two injectors were typically lower in comparison with those with the aeroramp injector at the same flow rates, and, consequently, no images are presented with the single-hole injector.

Instantaneous and frame-averaged OH-PLIF false-color images of the flame plume generated by the dc and ac torch are shown in Figs. 14–17. With the dc torch, the same camera configuration and gain settings were used. However, the OH-PLIF images employing the ac torch were recorded at a later time, and both the camera gain setting and field of view were somewhat different than that for experiments with the dc torch. To account for the differences in intensity, the relative camera gain was quantified, as was the differences of the fields of view between the two experiments. Based

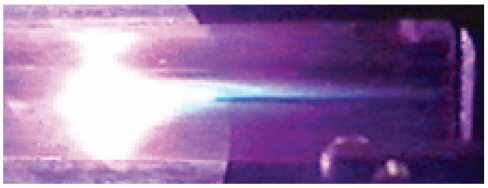

a) Single Hole (5.3 g/s, 318 K), Freestream (5.4 atm, 586K), AC Plasma Torch (5 kWPeak, 470 SLPM Air)

b) Aeroramp (5.4 g/s, 352 K), Freestream (5.4 atm, 592K), AC Plasma Torch (5 kWPeak, 470 SLPM Air)

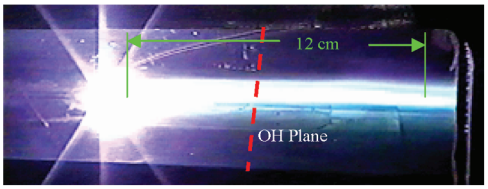

c) Aeroramp (5.2 g/s, 320 K), Freestream (5.4 atm, 588K), DC Plasma Torch (4.9±0.2 kWDC, 40 SLPM Air)

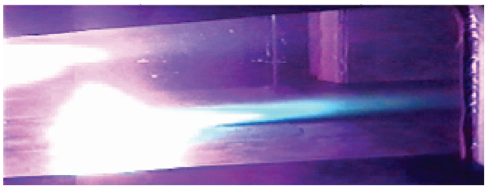

d) Aeroramp (5.4 g/s, 336 K), Freestream (5.4 atm, 586 K), DC Plasma Torch (4.0±0.1 kWDC, 40 SLPM N_2)

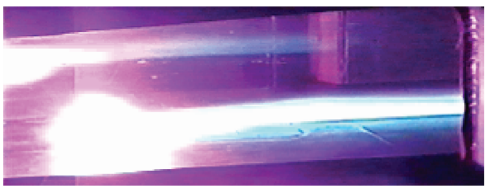

e) Aeroramp (3.3 g/s, 336 K), Freestream (5.4 atm, 586 K), DC Plasma Torch (4.0±0.1 kWDC, 40 SLPM N_2)

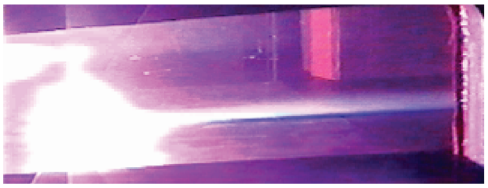

f) Aeroramp (3.4 g/s, 296 K), Freestream (5.4 atm, 305K), DC Plasma Torch (4.0±0.1 kWDC, 40 SLPM N_2)

Fig. 13 Video image of the ac and dc plasma torches (station 2) with an ethylene-fueled aeroramp injector upstream (not in view) in a Mach 2 flow. Flow is left to right, 12 cm from torch to downstream edge of insert.

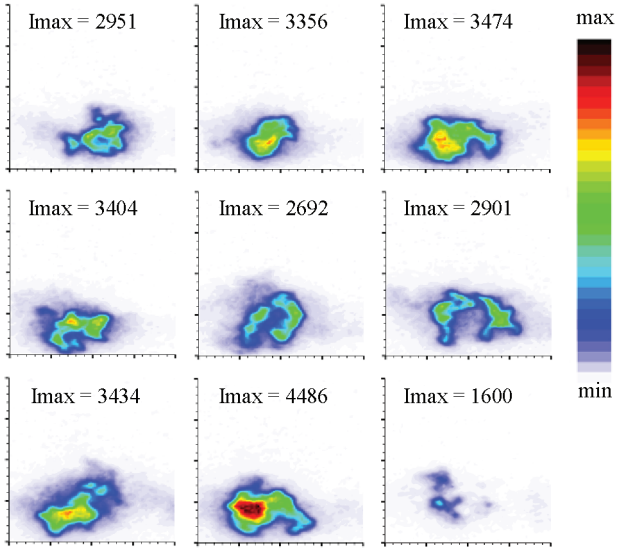

Fig. 14 False-color instantaneous OH-PLIF images with an aeroramp injector at 3.3 g/s and the dc plasma-torch igniter at station 1 using an N_2 feedstock at 40 SLPM and 4 kW input power. The laser sheet was positioned 5.1 cm downstream of the plasma torch. The maximum count is indicated on each frame.

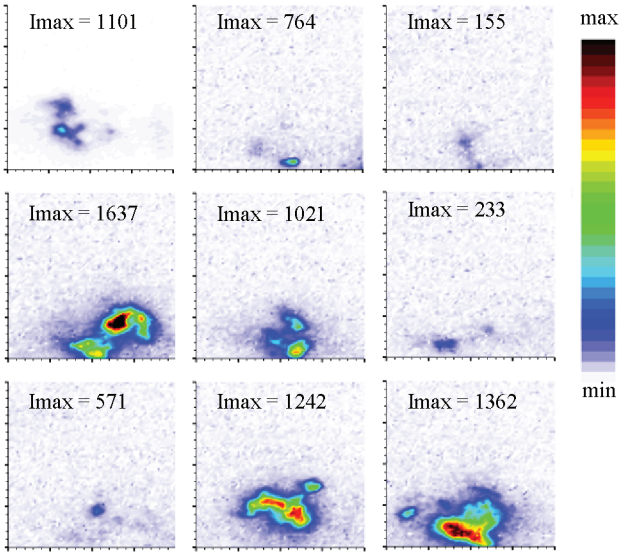

Fig. 15 False-color instantaneous OH-PLIF images with aeroramp injector at 5.3 g/s and the ac plasma-torch igniter at station 2 using a air feedstock at 235 SLPM and 5 kW input power. The laser sheet was positioned 5.1 cm downstream of the plasma torch. The maximum signal is indicated on each frame.

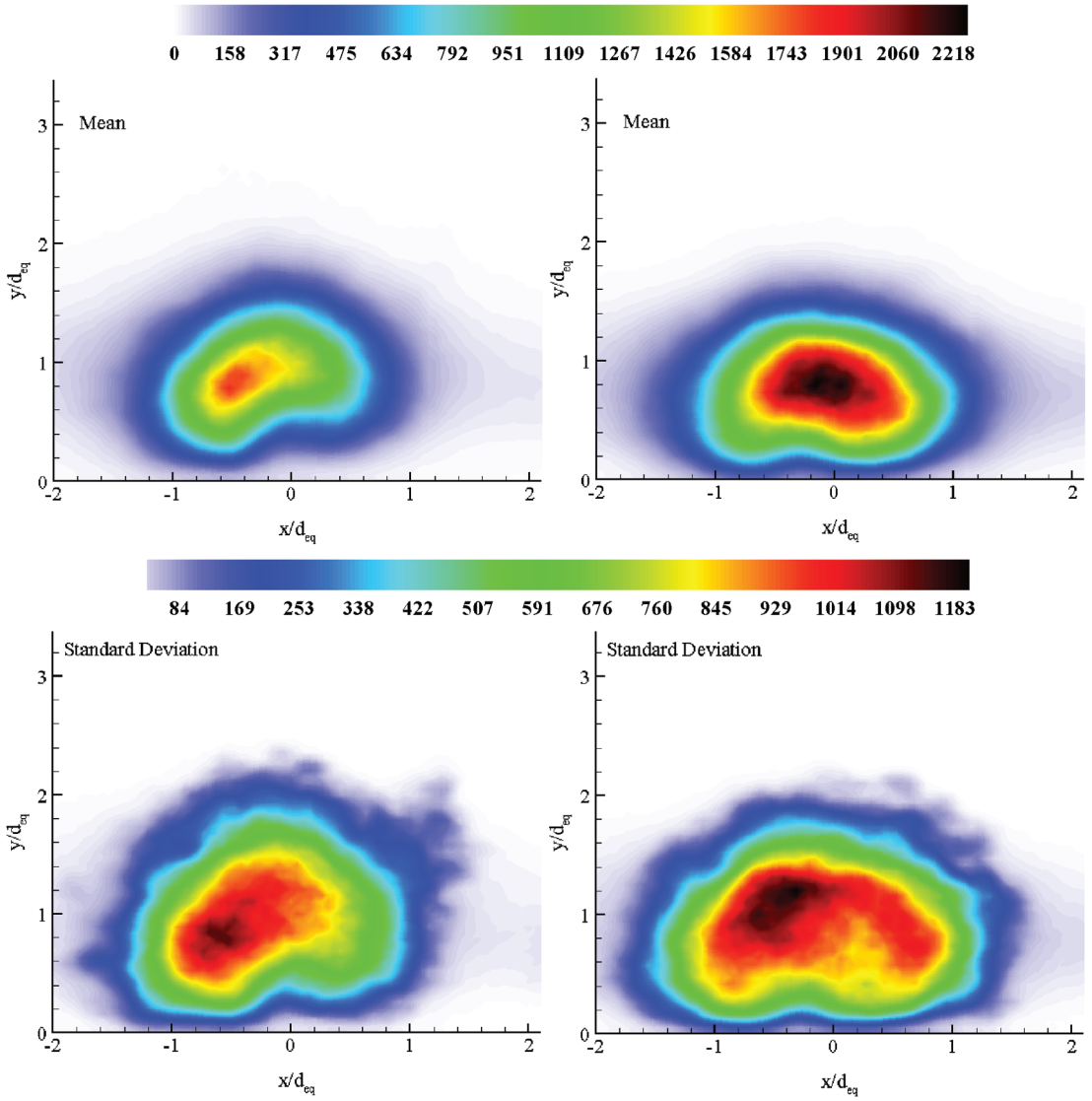

Fig. 16 False-color, average and standard deviation OH-PLIF images (300 image samples) with the aeroramp injector at 3.3 ± 0.1 g/s and the dc plasma-torch igniter using an N_2 feedstock at 40 SLPM and 4.0 ± 0.1 kW input power. Left: torch positioned at station 1. Right: torch positioned at station 2. The laser sheet was positioned 5.1 cm downstream of the torch station in both cases.

on these two factors, an intensity multiplier of 1.8 was applied to the ac torch OH-PLIF measurements.

The field of view in all images in Figs. 14–17 equals 4×4 equivalent injector diameters d_{eq}, (1.9 × 1.9 cm). The data presented were taken at a nominal freestream total temperature of 590 K and total pressure of 5.4 atm with a nominal fuel mass flow rate of 3.3 or 5.3 g/s (ethylene). These data were presented to show the slight difference in penetration of the flame plume created by placing the plasma torch closer to the aeroramp fuel injector; here, the plasma jet is enveloped into the fuel-plume counter-rotating axial-vortex pair. In general, the dimensions of the overall fuel plume were near the same width or larger than the region indicated in the images, and the flame plume was formed between two distinct fuel-jet cores.

The instantaneous images in Figs. 14 and 15, and standard deviation plots in Figs. 16 and 17 give an indication of the turbulent nature of the flowfield and the complex interaction of the fuel jet, the plasma jet, and the freestream air: significant reaction can take place only when a flammable fuel–air mixture interacts with a hot pocket of torch gas or products of combustion (from upstream). Consequently, the standard deviation of the OH signal is large and the average OH level is thus much reduced from the maximum instantaneous values. Trends in OH-PLIF intensity are presented in Figs. 18–20 and in Table 2. Figure 18 shows a plot of averaged image statistics as a function of input power for the dc plasma torch. Data in this figure were generated with the aeroramp injector and two torch stations at fuel flow rates of 5.3 and 3.3 g/s. During the experiments, this mean/median ratio of the image maximum intensity was used to indicate if the flame plume had crossed the laser sheet boundary. When the flame's downstream edge is near the boundary, the levels of OH vary strongly from one image to the next, as can be seen in the instantaneous images in Fig. 15. When the flame tip was close to the sheet, the median image deviated significantly from the mean image (300 image sample size). The flame was judged to be *through* the sheet when the decreasing mean/median ratio value approached unity. The typical trends seen with the dc torch at a 40 SLPM nitrogen feedstock flow rate were that the flame pushed through the boundary sooner at lower power levels at torch station 2 (vs 1) and at the lower fuel flow rate.

Plots of OH-PLIF mean image maximum intensity (top) and the mean of instantaneous image maximum intensities (bottom) are shown as a function of feedstock (nitrogen) flow rate in Fig. 19; here, the fuel flow rate and torch power were 3.3 g/s and 4 kW, respectively. The two averaging techniques show different ways of interpreting the PLIF image data. Because of the small size of the OH pockets relative to the area within which the pockets can fluctuate, the maximum of the mean image intensity was, in general, much lower than the average of the shot-to-shot maximum OH levels. In addition, this also created a rather large standard deviation throughout the plume area in the image (see Figs. 16 and 17). On evaluation of the shot-to-shot image maximums (Fig. 19, bottom

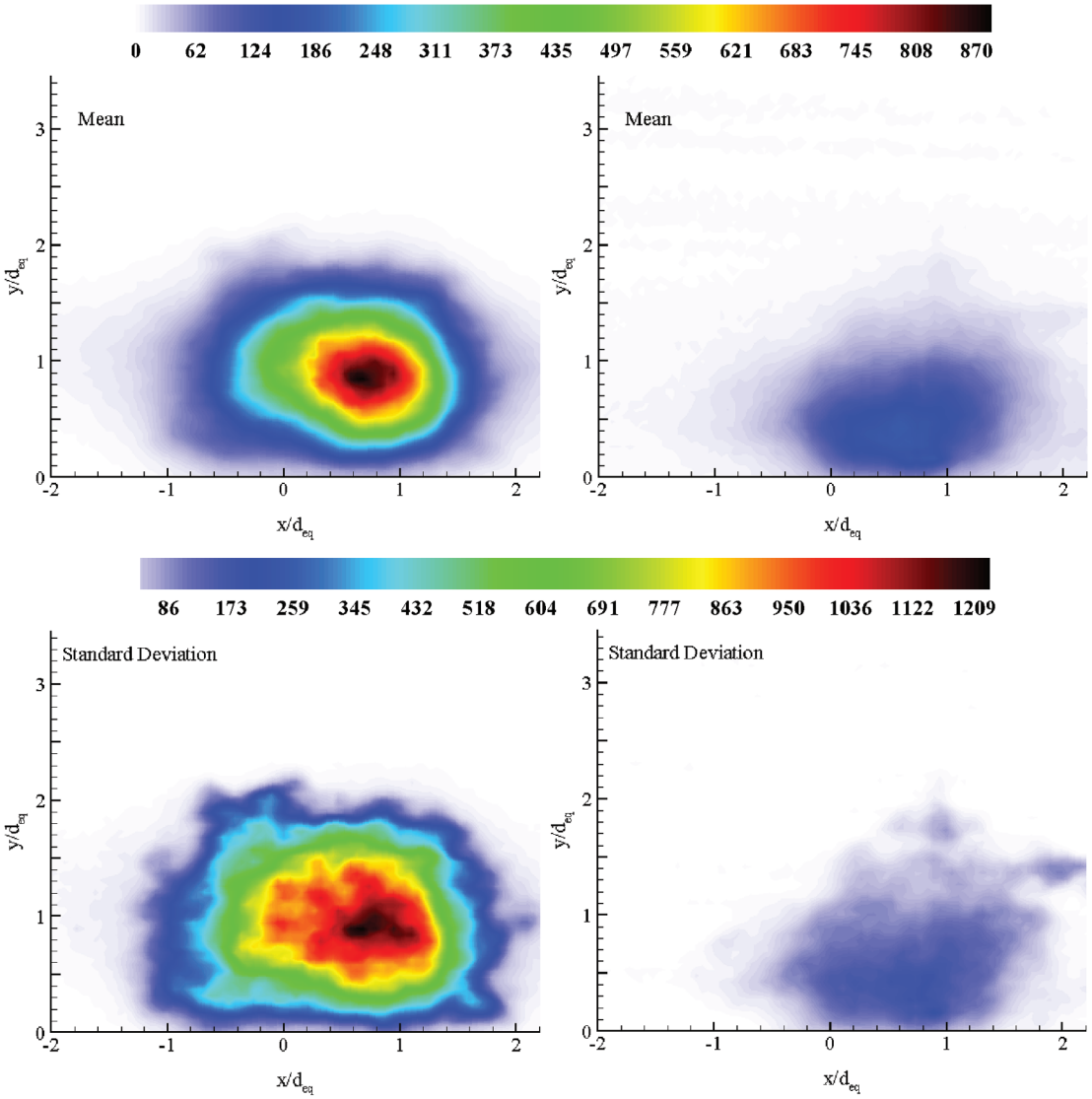

Fig. 17 False-color, average and standard deviation OH-PLIF images (100 image samples) with the aeroramp injector at 5.3 ± 0.1 g/s. Left: dc plasma-torch igniter using an air feedstock at 40 SLPM and 4.9 ± 0.2 kW input power. Right: ac plasma torch at 235 SLPM air and 5.0 ± 0.2 kW. Both torches are positioned at station 2. The laser sheet was positioned 5.1 cm downstream from torch station.

plot), it is apparent that maximum OH intensity levels produced at both stations were comparable for the feedstock flow rates presented.

A comparison of the mean OH maximum intensity levels for a range of parameters (torches, flow rates, and stations) is presented in Fig. 20. Most of the dc-torch data are with a nitrogen feedstock at a 40 SLPM flow rate with the exception of the three marked data points on the graph. Of these points, two show the data with the dc torch in operation with an air feedstock. The ac-torch OH intensity data correspond to a 235 SLPM air feedstock flow rate. The typical trends in the graph show that the mean OH instantaneous maximum intensity increased with input power and decreased with higher fuel flow rate levels. The standard deviation values were typically higher at the upstream torch station (station 1) with the dc torch and were particularly high with the torch in operation with air or at high power. In general, the dc torch produced a higher level of OH than the ac torch. A comparison of the dc torch in operation with air and nitrogen feedstocks shows, for the limited amount of data available, that the performance of the dc torch with air feedstock was similar to that with nitrogen. Also, it is interesting to note that the OH-PLIF intensity is higher at lower feedstock flow rates.

A preliminary experiment was also performed using aerated-liquid JP-7 (nitrogen as the aerated gas) with the plasma-torch igniter. In general, the flame plume was not as long as with gaseous ethylene and propagation of the flame down the full length of the tunnel was not achieved. It was also found that the JP-7 fuel fluoresced with 283 nm excitation. However, the OH-PLIF signal was typically several times that of the JP-7 at a fuel flow rate of 2 g/s. With increasing fuel flow rate, the OH-PLIF decreased (consistent with results with ethylene), whereas that of the fuel increased. Based on the preliminary data, it is expected that the aerated-liquid JP-7 will require a higher plasma-torch power relative to that required for ethylene to achieve a flame that propagates down the length of the combustor. However, use of an air plasma and/or different aerating gases may enhance the size of the flame.

Summary and Conclusions

By learning to simulate a plasma torch in a quiescent environment and the combined plasma torch and fuel jet in a supersonic crossflow, it is hoped that a more fundamental understanding of the ignition and flame spreading process will be achieved. Computational modeling of the plasma torch that encompasses the dynamic mechanisms involved in arc heating and combustion must be developed. Because of the fluctuating nature of the plasma arc, average values, such as bulk temperature, can be misleading; clearly, pockets of hot, highly excited, and ionized gas can have a significant influence on the ignition and combustion processes. With this understanding, further computational modeling of the ignition process in a full-configuration scramjet combustor must take this into account to

Table 2 OH-PLIF image statistics for data points in Fig. 20

Torch and location	C_2H_4 fuel flow rate, g/s	Plasma torch			PLIF	Averaged image statistics				Instantaneous image statistics	
		Power, kW	Feedstock	Flow rate, SLPM	images	Max, μ, AU	M, μ/median, AU	σ@ max, AU	μ(max), AU	μ(M)/median(M), AU	σ(max), AU
dc, S#1	5.4 ± 0.1	8.2 ± 0.1 kW	Air	20	100	920	1.67	962	2849	0.98	972
	5.3 ± 0.1	7.0 ± 0.1 kW	N_2	40	300	656	2.39	885	2348	0.91	1253
	5.3 ± 0.1	4.1 ± 0.1 kW	N_2	40	300	187	3.53	503	605	3.81	871
	3.3 ± 0.1	4.0 ± 0.1 kW	N_2	40	300	1834	0.98	1150	3074	0.95	774
	3.3 ± 0.1	4.0 ± 0.1 kW	N_2	20	300	2261	0.94	1032	4050	0.98	488
ac, S#1	5.3 ± 0.1	5.0 ± 0.2 kW	Air	235	100	48	48/0	321	450	1.74	458
	3.3 ± 0.1	5.0 ± 0.2 kW	Air	235	100	541	2.62	769	2086	0.98	717
dc, S#2	5.2 ± 0.2	4.9 ± 0.2 kW	Air	40	100	1532	1.13	1156	2584	1.04	1295
	5.3 ± 0.1	4.0 ± 0.1 kW	N_2	40	300	266	1.87	457	1017	1.43	864
	3.4 ± 0.1	6.3 ± 0.1 kW	N_2	40	300	3549	0.95	982	4595	1.00	455
	3.3 ± 0.1	4.0 ± 0.1 kW	N_2	40	300	2261	0.92	1012	3587	0.96	682
ac, S#2	5.3 ± 0.1	5.0 ± 0.2 kW	Air	235	100	313	1.03	363	954	1.01	412
	3.3 ± 0.1	5.0 ± 0.2 kW	Air	235	100	1005	0.95	721	1684	0.85	717

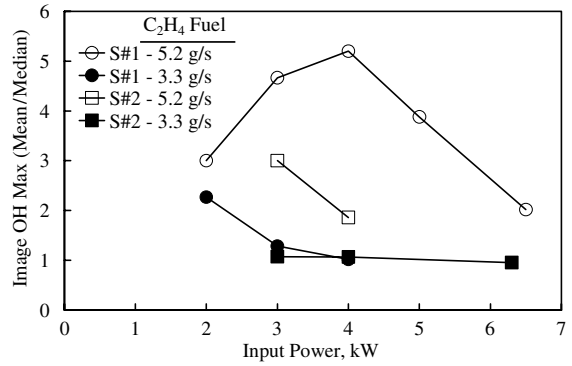

Fig. 18 Flame boundary indicator (mean/median) at stations 1 (S#1) and 2 (S#2). Aeroramp injector, dc torch, N_2 feedstock, 40 SLPM.

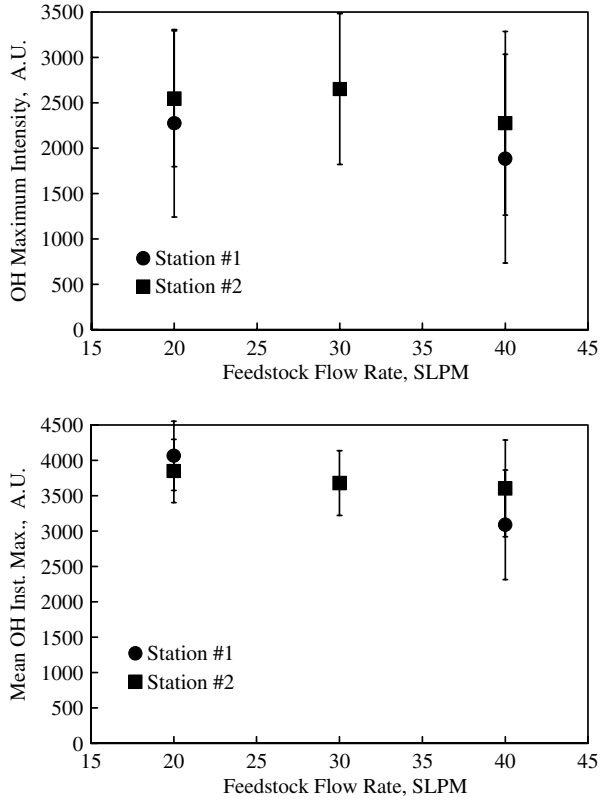

Fig. 19 OH-PLIF mean image maximum intensity (left) and mean of instantaneous image maximums (right) as a function of feedstock flow rate. Data generated with aeroramp injector at, nominally, 3.3 g/s and the dc torch using an N_2 feedstock at 40 SLPM and nominal 4 kW input power.

create a more robust computational design tool for the simulation of plasma-assisted ignition.

The primary reason for conducting this work was to further our understanding of the ignition process in a small-scale scramjet duct. Our current research combustors, however, incorporate a cavity flame holder into the flow path. Clearly, the cavity is an effective flame holder but also appears to aid in ignition: Mathur et al. [19], for example, achieved ignition with only a spark plug located within the cavity flame holder. It is believed that, to sustain combustion at Mach 4, a minimum equivalence ratio of about 0.25 is required [19], a value corresponding to several grams per second (per injector with 4 injectors) of ethylene or JP-7 at the Mach 4 condition with total temperatures and pressures of 900 K and 5.4 atm, respectively. Of course, with ethylene fuel at 5.4 g/s, the dc plasma torch has established a long flame (at 590 K total temperature) at 4 kW total input power level. However, it appears that more torch power (than necessary with ethylene) may be required to obtain ignition in a less

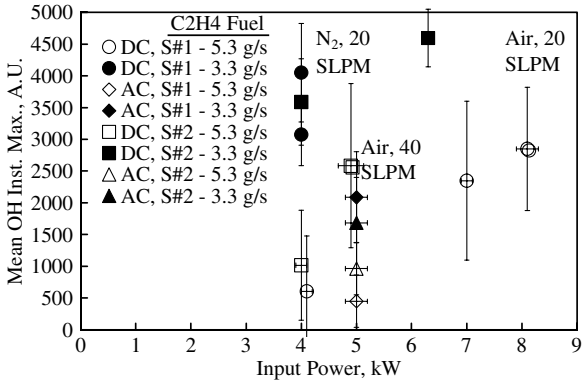

Fig. 20 Mean OH instantaneous maximum intensity comparison for the aeroramp injector with the dc and ac plasma torches at both downstream torch stations (S#1 and S#2) as a function of total input power. The laser sheet was positioned 5.1 cm downstream of the plasma-torch orifices. With the dc torch, the feedstock is N_2 at 40 SLPM, unless specified. With the ac torch, the feedstock is air at 235 SLPM.

reactive fuel such as JP-7, as is also suggested by the experiments performed by Northam et al. [2] with methane as the combustor fuel.

It is noted that engine scale and/or geometry will, presumably, play a significant role in the power required for plasma-assisted ignition in a scramjet. For example, a round scramjet with flush-wall fuel injectors and a cavity flame holder might require a higher level of input power for ignition, due to the lack of the low-momentum flow in the corners of rectangular ducts; however, the ease with which ignition is achieved may also depend on the volume of the cavity flame holder and thus on the engine scale. Ultimately, configurations that can capitalize on the generation of power (to initiate ignition) through fuel heat release (such as a microburner [13] or a well-placed plasma torch) will not increase in size as dramatically as one that is dependent on electrical power alone.

Finally, some comment on defining constraints is appropriate and, indeed, necessary. The initial constraints for concept comparison and evaluation in this study have been defined by igniter size and energy/power consumed. Of course, additional systems-type constraints will need to be introduced to select a particular ignition strategy for a particular engine. The constraint on igniter size is based on the physical access to the test hardware. For the engine described by Mathur et al. [19], with the configuration shown in Fig. 2, the space between injectors limits the torch size to about 3 cm, and a size approaching 2 cm is preferable; at larger engine scales, the torch size could naturally be increased. The energy constraints of the plasma ignition devices are defined by short pulse (ignition) and a steady-state (flame-holding) operation. The CFD simulations imply that ignition can be accomplished in the span of a few milliseconds; the energy required for, say, 10 ms of torch operation, is then 10 s of Joules, an amount small compared to the capacity of a reasonably sized battery. If, however, torches were used for flame holding for an engine of the scale described by Mathur et al. [19], then, presumably, either power consumption would need to be reduced (to perhaps 100 s of Watts on average) or a power generation method (e.g., magnetohydrodynamic, MHD, power generation) would be needed. Again, this constraint could, presumably, be progressively relaxed with increases in the vehicle size.

The main goal of this plasma ignition effort is to asses the prospect of main-fuel ignition with plasma-generating devices in a supersonic flow. As the study progresses, baseline conditions of operation are being established, such as the required operational time of the device to initiate a combustion shock train. The torches in use in this study employ different methods of introducing plasma energy into a fueled, supersonic crossflow. Not only do they differ in the duration of their plasma (dc vs ac), they also differ substantially in orifice geometry and thus the range of feedstock mass flow rate. However, both torches are realistic in size and operate within reasonable power constraints with the ac torch operating with an average power of approximately 200 W.

To compare the potential of each concept, an understanding of the flow physics of each part of the system (separate and together) is being achieved. Both the dc- and ac-powered plasma torches were investigated individually in a quiescent environment to gain insight into the basic operational flow features of the devices. To understand the constraints involved with the ignition process, an experimental effort to study the coupling of nitrogen/air plasma jets with a gaseous (ethylene) or liquid (JP-7) hydrocarbon fuel stream was accomplished. Results from the individual igniter studies have shown the plasma igniters to produce hot pockets of gas with peak temperatures above 5000 K. Ethylene and JP-7 fueled flames were also produced in a Mach 2 supersonic flow with a total temperature and pressure of 590 K and 5.4 atm, respectively. Results from these studies suggest that the dc torch was more effective in producing a flame than the ac torch for similar levels of input peak power for the configurations tested. Furthermore, both air and nitrogen feedstocks produced comparable results; OH production from the dc torch operated with an air feedstock was somewhat greater, but the difference was well within the respective standard deviations. Of course, this is not too surprising, because most of the air for combustion must come from main duct flow.

As the constraints involved with the ignition process are further understood, this, in turn, will help evolve the design and use of the igniters and may also serve as a baseline against which to test new igniter concepts. Finally, a more fundamental understanding of an alternative to existing starting methods, such as those based on silane or a gas generator, is being established; this alternative does not involve the use of toxic (and dangerous) chemicals, is reusable (allowing restart attempts), and is capable of being integrated into the next generation of hydrocarbon-fueled scramjet applications.

Acknowledgments

We thank the following people for their contributions to the plasma-assisted ignition effort at the U.S. Air Force Research Laboratory: Joseph Schetz and Walter O'Brien (Virginia Polytechnic Institute and State University); Greg Elliot and Martin Boguzko (University of Illinois); Jim Crafton, Mark Hsu, Bill Terry, Dave Schomer, and Gary Streby (Innovative Scientific Solutions, Inc.); K.-C. Lin, (Taitech, Inc.); Paul Kennedy (U.S. Air Force Research Laboratory, Propulsion Directorate); Andrew Dwenger (GoHYPERSONIC, Inc.).

References

[1] Kimura, I., Aoki, H., and Kato, M., "Use of a Plasma Jet for Flame Stabilization and Promotion of Combustion in Supersonic Air Flows," *Combustion and Flame*, Vol. 42, No. 3, Sept. 1981, pp. 297–305. doi:10.1016/0010-2180(81)90164-4

[2] Northam, G., McClinton, C., Wagner, T., and O'Brien, W., "Development and Evaluation of a Plasma Jet Flameholder for Scramjets," AIAA Paper 84-1408, June 1984.

[3] Wagner, T., O'Brien, W., Northam, G., and Eggers, J., "Plasma Torch Igniter For Scramjets," *Journal of Propulsion and Power*, Vol. 5, No. 5, 1989, pp. 548–554.

[4] Kanda, T., Hiraiwa, T., Mitani, T., Tomioka, S., and Chinzei, N., "Mach 6 Texting of a Scramjet Engine Model," *Journal of Propulsion and Power*, Vol. 13, No. 4, 1997, pp. 543–551.

[5] Fuji, S., Shuzenji, K., Kato, R., and Tachibana, T., "Augmentation of Ignition Arcs for Air Breathing Combustion by Teflon Sublimates," AIAA Paper 1998-3215, July 1998.

[6] Jacobsen, L. S., Gallimore, S. D., Schetz, J. A., and O'Brien, W. F., "Integrated Aeroramp Injector/Plasma-Igniter for Hydrocarbon Fuels in a Supersonic Flow, Part A: Experimental Studies of the Geometrical Configuration," AIAA Paper 2001-1766, April 2001.

[7] Gallimore, S. D., Jacobsen, L. S., O'Brien, W. F., and Schetz, J. A., "Integrated Aeroramp Injector/Plasma-Igniter for Hydrocarbon Fuels in a Supersonic Flow, Part B: Experimental Studies of the Operating Conditions," AIAA Paper 2001-1767, April 2001.

[8] Williams, S., Arnold, S., Bench, P., Viggano, A., Dotan, I., Midey, A., Morris, T., Morris, R., Maurice, L., and Sutton, E., "Potential Enhancement of Hydrocarbon Fueled Combustor Performance Via Ionization," *XIV ISABE International Symposium on Air Breathing Engines*, AIAA, Reston, VA, 1999.

[9] Sato, Y., Sayama, M., Ohwaki, K., Masuya, G., Komuro, T., Kudou, K., Murakami, A., Tani, K., Wakamatsu, Y., Kanda, T., Chinzei, N., and Kimura, I., "Effectiveness of Plasma Torches for Ignition and Flameholding in Scramjet," AIAA Paper 89-2564, July 1989.

[10] Masuya, G., Kudou, K., Komuro, T., Tani, K., Kanda, T., Wakamatsu, Y., Chinzei, N., Sayama, M., Ohwaki, K., and Kimura, I., "Some Governing Parameters of Plasma Torch Igniter/Flameholder in a Scramjet Combustor," *Journal of Propulsion and Power*, Vol. 9, No. 2, 1993, pp. 176–181.

[11] Tomioka, S., Hiraiwa, T., Sakuranaka, N., Murakami, A., Sato, K., and Matsui, A., "Ignition Strategy in a Model Scramjet," AIAA Paper 96-3240, July 1996.

[12] Masuya, G., Takita, K., Sato, T., Ohwaki, K., Takahashi, K., Uemoto, T., Ju, Y., and Matsumoto, M., "Ignition of Parallel and Low Angle Hydrogen Jet by Plasma Torch," *XIV ISABE International Symposium on Air Breathing Engines*, AIAA, Reston, VA, Sept. 1999.

[13] Kobayashi, K., Tomioka, S., and Mitani, T., "Ignition by an H_2/O_2-Microburner in a Supersonic Flow," AIAA Paper 2001-1763, April 2001.

[14] Shuzenji, K., Kato, R., and Tachibana, T., "Two-Stage Plasma Torch Ignition in Supersonic Airflows," AIAA Paper 2001-3740, July 2001.

[15] Masuya, G., Choi, B., Ichikawa, N., and Takita, K., "Mixing and Combustion of Fuel Jet in Pseudo-Shock Waves," AIAA Paper 2002-0809, Jan. 2002.

[16] Bonanos, A, M., Sanders, D. D., Schetz, J. A., and O'Brien, W. F., "Hot-Flow Testing of an Integrated Aero-Ramp Injector/Plasma-Igniter for Scramjets with Hydrogen and Hydrocarbon Fuels," AIAA Paper 2005-3425, May 2005.

[17] Bonanos, A, M., Schetz, J. A., O'Brien, W. F., and Goyne, C. P., "Scramjet Operability Studies of a Multifuel Integrated Aeroramp Injector/Plasma Igniter," AIAA Paper 2003-6987, Dec. 2003.

[18] Pandolfini, P. P., Billig, F. S., Corpening, G. P., Corda, S., and Friedman, M. A., "Analyzing Hypersonic Engines Using the Ramjet Performance Analysis Code," *APL Technical Review*, Vol. 2, No. 1, 1990, pp. 68–79.

[19] Mathur, T., Streby, G., Gruber, M., Jackson, K., Donbar, J., Donaldson, W., Jackson, T., Smith, C., and Billig, F., "Supersonic Combustion Experiments with a Cavity-Based Fuel Injector," AIAA Paper 99-2102, June 1999.

[20] White, J. A., and Morisson, J. H., "Pseudo-Temporal Multi-Grid Relaxation Scheme for Solving the Parabolized Navier-Stokes Equations," AIAA Paper 99-3360, June 1999.

[21] Edwards, J. R., "Low Diffusion Flux-Splitting Scheme for Navier–Stokes Calculations," *Computers and Fluids*, Vol. 26, No. 6, 1997, pp. 635–659.
doi:10.1016/S0045-7930(97)00014-5

[22] Baurle, R. A., Mathur, T., Gruber, M. R., and Jackson, K. R., "Numerical and Experimental Investigation of a Scramjet Combustor for Hypersonic Missile Applications," AIAA Paper 98-3121, July 1998.

[23] Liu, J., Tam, C.-J., Lu, T., and Law, C., "Simulations of Cavity-Stabilized Flames in Supersonic Flows Using Reduced Chemical Kinetic Mechanisms," AIAA Paper 2006-4862, 2006.

[24] Jacobsen, L. S., Carter, C. D., Jackson, T. A., Schetz, J. A., O'Brien, W. F., Boguzko, G. S., Elliott, M., and Crafton, J. W., "Experimental Investigation of a DC Plasma-Torch Igniter," AIAA Paper 2002-5228, Sept. 2002.

[25] Kuo, S. P., Koretzky, E., and Orlick, L., "Design and Electrical Characteristics of a Modular Plasma Torch," *IEEE Transactions on Plasma Science*, Vol. 27, No. 3, 1999, pp. 752–758.
doi:10.1109/27.774679

[26] Behbahani, H., Fontijn, A., Mueller-Dethlefs, K., and Weinberg, F., "Destruction of Nitric Oxide by Nitrogen Atoms from Plasma Jets," *Combustion Science and Technology*, Vol. 27, Nos. 3–4, 1982, pp. 123–132.
doi:10.1080/00102208208946981

[27] Jacobsen, L. S., Gallimore, S. D., Schetz, J. A., and O'Brien, W. F., "Improved Aerodynamic Ramp Injector in Supersonic Flow," AIAA Paper 2001-0518, Jan. 2001.

R. Bowersox
Associate Editor